Escherichia coli chemotaxis is information limited

H. H. Mattingly[1,2,5], **K. Kamino**[1,2,5], **B. B. Machta**[3,4 ✉] **and T. Emonet**[1,2,3 ✉]

Organisms acquire and use information from their environment to guide their behaviour. However, it is unclear whether this information quantitatively limits their performance at behavioural tasks. Here we relate information to the ability of *Escherichia coli* to navigate up chemical gradients, the behaviour known as chemotaxis. First, we derive a theoretical limit on the speed with which cells climb gradients, given the rate at which they acquire information. Next, we measure cells' gradient-climbing speeds and the rate of information acquisition by their chemotaxis signalling pathway. We find that *E. coli* cells make behavioural decisions with much less than the one bit required to determine whether they are swimming up the gradient. Some of this information is irrelevant to gradient climbing, and some is lost in communication to behaviour. Despite these limitations, *E. coli* cells climb gradients at speeds within a factor of two of the theoretical bound. Thus, information can limit the performance of an organism, and sensory–motor pathways may have evolved to efficiently use information acquired from the environment.

Organisms' survival depends on their ability to perform behavioural tasks. These tasks require that organisms measure signals in their environments and respond appropriately. Information theory is a natural language for quantifying the fidelity of measurements and responses, but it is unclear how an abstract quantity like information might limit performance in real-world tasks. Past studies have used information theory to understand the maximum amount of information that biological systems can acquire and transmit about environmental signals[1–6] and have shown that they can approach biophysical limits[6–9]. However, high information transfer is not sufficient for high performance because not all information contained in the signal is relevant (that contributes to performing the task) and not all of it is appropriately acted on by the organism[10]. What limits does information place on performance, and how efficiently do organisms use the information they acquire relative to these limits?

We address these questions using one of the best-understood behaviours in biology: bacterial chemotaxis. The bacterium *Escherichia coli* alternates between 'runs' (which propel the cell forward) and 'tumbles' (which randomly reorient its swimming direction)[11] (Fig. 1). *E. coli* bacteria continuously sense the concentration $c(t)$ of the chemoattractant they encounter using transmembrane receptors. Relative changes in concentration[12], namely, $s(t) = \frac{d}{dt} \log(c)$, which we define as the 'signal', induce changes in activity $a(t)$ of the receptor-associated CheA kinases. Thus, CheA kinase activity encodes *E. coli*'s estimate of the signal. CheA activity then modulates transitions in the cell's swimming behaviour $m(t)$ between the run and tumble states via a signal transduction pathway[13,14]. If the attractant concentration is increasing ($s(t) > 0$), the cell—on average—runs longer, thereby biasing its random motion up the gradient[11]. However, noise in sensing and signal transduction corrupt the signal[15–18]. Since the goal of chemotaxis is to climb chemical gradients, we quantify performance as the cell's drift velocity v_d up a static gradient. *E. coli* chemotaxis has been extensively studied, but how much information a cell acquires about chemical signals[19–22] and its relationship to chemotactic performance are unknown.

To efficiently use information, a cell must only encode information in CheA that is relevant to gradient climbing and appropriately act on that information at the motors to guide behaviour. An inef-

ficient cell may acquire abundant information about the signal, but it is either irrelevant to chemotaxis or goes unused. To determine how efficiently *E. coli* bacteria use information to navigate, we must first derive the maximum gradient-climbing speed that a cell can achieve given the amount of information available in CheA. Second, we need to quantify how close to this theoretical bound *E. coli* cells operate by measuring the amount of information available in CheA as well as the cells' performance with that information (Fig. 1c). Consequently, we will quantify information transfer on two different length scales: the information about signals available in the kinase activity and the information used to perform behaviours.

To do this, we must define a measure of information acquisition. Bacteria continuously encode the chemical signals they experience. Thus, unlike most studies of biological systems[1–3,5,6], we cannot use the one-shot mutual information[23] between signal $s(t)$ and kinase activity $a(t)$ as a measure of information transfer, because it is blind to past signals experienced by the cell. Instead, we need to quantify information transfer between the signal and kinase trajectories; in this case, we use a steady-state information rate[24]. Furthermore, signals are generated by the cell's own motion in the gradient[25]. This makes a natural extension—the mutual information rate $\dot{MI}(s;a)$ between $s(t)$ and $a(t)$—also unsuitable, because kinase activity and signal are correlated even for cells that do not respond to the signal (Fig. 1a,b). We address these challenges by decomposing the mutual information rate into the sum of two directed information terms (Supplementary Section 1 and refs. [26,27]): the transfer entropy[21,28] rates from kinase activity to signal $\dot{I}_{a \to s}$ and from signal to kinase activity $\dot{I}_{s \to a}$, or $\dot{MI}(s;a) = \dot{I}_{a \to s} + \dot{I}_{s \to a}$. The first term $\dot{I}_{a \to s}$ quantifies the feedback of kinase activity onto signal via the behaviour. The second term $\dot{I}_{s \to a}$ measures the influence of the signal on kinase activity (in bits s⁻¹) and must be non-zero for the cell to climb the gradient.

Next, we need to derive the theoretical limit on gradient-climbing performance v_d imposed by information $\dot{I}_{s \to a}$. The drift speed depends on how the cell's motors use information about past signals that is provided by CheA. Although information at the motors $\dot{I}_{s \to m}$ cannot exceed the information in kinase activity $\dot{I}_{s \to a}$ (ref. [29]), at best, all the information in the kinase activity is preserved at the motors, in which case $\dot{I}_{s \to m} = \dot{I}_{s \to a}$. Therefore, to derive the bound, we sought to determine how $\dot{I}_{s \to m}$, and thus $\dot{I}_{s \to a}$, bounds performance v_d.

¹Department of Molecular, Cellular, and Developmental Biology, Yale University, New Haven, CT, USA. ²Quantitative Biology Institute, Yale University, New Haven, CT, USA. ³Department of Physics, Yale University, New Haven, CT, USA. ⁴Systems Biology Institute, West Campus, Yale University, New Haven, CT, USA. ⁵These authors contributed equally: H. H. Mattingly, K. Kamino. ✉e-mail: benjamin.machta@yale.edu; thierry.emonet@yale.edu
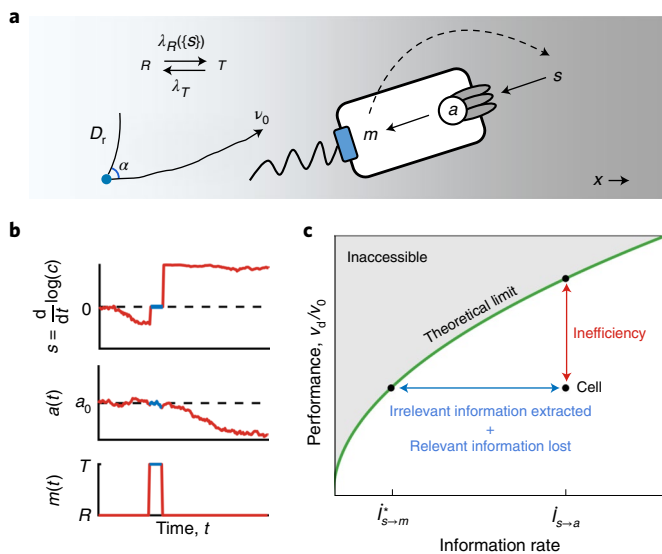
Fig. 1 | Information sets an upper limit on chemotaxis performance.
a, In our model, a cell navigates chemical gradients by sensing relative changes $s(t) = \frac{d}{dt} \log(c)$ in attractant concentration c over time t using receptors, which influence the activity a of receptor-associated kinases. Here a encodes *E. coli*'s estimate of the signal. Then, a modulates stochastic transitions between behavioural states m: a run state R, in which the cell swims with constant speed v_0 and rotational diffusion D_r; and a tumble state T, in which it randomly reorients with directional persistence α (Supplementary Fig. 1). Responses to past signals $\{s\}$ that are transduced from a to m are described by changes in the cell's transition rate $\lambda_R(\{s\})$ from the run to tumble states. The cell's motion creates the signal that it experiences (dashed arrow). **b**, Signals experienced by the cell, $s(t)$ (top), are encoded in noisy kinase activity $a(t)$ (middle), which influences the stochastic behavioural state transitions $m(t)$ (bottom). The flow of information from $s(t)$ to $a(t)$ and from $a(t)$ to $m(t)$ implies that $\dot{I}_{s \to a} \geq \dot{I}_{s \to m}$. **c**, Given the information rate $\dot{I}_{s \to a}$, there is an upper limit on the chemotaxis performance (green line), defined as the cell's up-gradient drift speed v_d relative to v_0 (equation (1)). The cell's performance is ultimately set by how much relevant information contained in $\dot{I}_{s \to a}$ is communicated to its behaviour, quantified by $\dot{I}^*_{s \to m}$. Real cells cannot reach the limit because of two factors (quantified by the length of the blue line): some of the information they encode in the CheA kinase activity is irrelevant for climbing the gradient, and some of the relevant information in a is lost during transfer to the motors m. These factors result in reduced performance (quantified by the length of the red line) and reduced efficiency of information usage.

To do this, we constructed a mathematical model of run-and-tumble navigation (Fig. 1a and Supplementary Section 2). During runs, cells swim with a constant speed v_0 and lose direction with rotational diffusion coefficient D_r. During tumbles, they randomly reorient with directional persistence α. In the absence of a gradient, cells switch from run to tumble and vice versa with rates λ_{R0} and λ_T, respectively. The fraction of time that the cell spends running is $P_{\text{run}} = \frac{\lambda_T}{\lambda_{R0} + \lambda_T}$. In shallow gradients, like those considered here, the tumble rate $\lambda_R(\{s\})$ depends approximately linearly on the history of signals experienced $\{s\}$ (refs. [30–33]).

Using the model above, we derived how v_d and $\dot{I}_{s \to m}$ depend on the behavioural response $\lambda_R(\{s\})$. Although any response to the signal implies information transfer, it does not imply a high drift speed. To find the limit, we derived the maximum drift speed v_d possible given the information rate $\dot{I}_{s \to m}$ by optimizing over responses $\lambda_R(\{s\})$. This revealed that the optimal behavioural response only depends on the

current rate of change of log concentration, $s(t)$ (Supplementary Section 4). Thus, information about the current signal is relevant to gradient climbing (Supplementary Section 5). Bacteria cannot implement the optimal behavioural response because they must make comparisons of concentrations over a finite time to infer $s(t)$ (ref. [15]). Nevertheless, the performance achieved by any behavioural response is bounded by the following (Fig. 1c):

$$v_d/v_0 \leq f(\theta) \left(\frac{\log(2)\ \dot{I}_{s \to a}}{12\ D_r} \right)^{1/2},$$

$$\text{where } 0 \leq f(\theta) \leq 1, \theta = \{\lambda_{R0}, P_{\text{run}}, \alpha\}, \tag{1}$$

where $\dot{I}_{s \to m} \leq \dot{I}_{s \to a}$ and $f(\theta) = \frac{(1-\alpha)\lambda_{R0}}{(1-\alpha)\lambda_{R0} + 2D_r} \left(8 \frac{D_r}{\lambda_{R0}} P_{\text{run}} \right)^{1/2}$. This expression makes rigorous the intuition that information transfer sets a limit on chemotaxis performance[15,20,22,24,34,35]. Out of the information contained in $\dot{I}_{s \to a}$, the amount that is both relevant and transferred to behaviour, $\dot{I}^*_{s \to m}$, ultimately determines the performance: $v_d/v_0 = f(\theta) \left(\frac{\log(2)\ \dot{I}^*_{s \to m}}{12\ D_r} \right)^{1/2}$ (Supplementary Section 5). Thus, the green line in Fig. 1c directly maps a cell's performance to $\dot{I}^*_{s \to m}$. Furthermore, the length of the blue line in Fig. 1c measures the amount of irrelevant information encoded in CheA plus the amount of relevant information lost in communicating to the motors. These factors lower the cell's performance relative to the theoretical limit by an amount quantified by the length of the red line. With this, we define the efficiency of information usage as the cell's actual drift speed relative to the maximum possible speed with the information available in CheA, that is,

$$\eta = \frac{v_d}{v_0} / \left[f(\theta) \left(\frac{\log(2)\ \dot{I}_{s \to a}}{12\ D_r} \right)^{1/2} \right] = \left(\dot{I}^*_{s \to m} / \dot{I}_{s \to a} \right)^{1/2}.$$

We next set out to measure how efficiently *E. coli* cells use information to navigate, η. First, we quantified the bound by measuring the rotational diffusion coefficient D_r and behavioural parameters θ from trajectories of swimming *E. coli* (Supplementary Figs. 1 and 2). Individual cells in a clonal population exhibit non-genetic differences in behavioural parameters[36–39], which—in *E. coli*—are highly correlated with P_{run} (refs. [36,38]). From these data, we find $f(\theta) = 0.531 \pm 0.005$ for cells with the median P_{run} ($\pm$one standard error throughout; Supplementary Table 1). This quantifies the minimum amount of information needed to climb a gradient. Surprisingly, the bound predicts that run-and-tumble navigation is theoretically possible with very small information rates: a hundredth of a bit per second is sufficient to climb gradients at ~6% of the run speed. This is far less than the one bit per run (~1 bit s^{-1}) required to distinguish whether concentration is currently increasing or decreasing before every tumble decision[24].

To compare *E. coli* with the theoretical limit, we measured the rate at which cells encode information about signals in their CheA kinase activity, $\dot{I}_{s \to a}$, during chemotaxis. Directly measuring the kinase activity in individual swimming cells is infeasible. Instead, we quantified the mutual information rate[24,40] between signal and kinase activity, $\dot{MI}(s;a)$, in immobilized cells by measuring their kinase response and noise properties and by separately measuring the signal statistics that they would experience during navigation (Fig. 2a). In these immobilized cells, $\dot{MI}(s;a) = \dot{I}_{s \to a}$ since there is no feedback of kinase activity onto the signal. Here $\dot{I}_{s \to a}$ quantified in this way in immobilized cells differs from $\dot{I}_{s \to a}$ in a swimming cell because it does not take into account higher-order correlations between s and a. However, these correlations contribute terms that are multiplied by higher powers of the gradient steepness $g = \frac{d}{dx} \log(c)$ and thus can be neglected in shallow gradients (Supplementary Section 8).

The signal statistics are characterized by their power spectrum $S(\omega)$. It is often difficult to know the natural signal statistics an organism experiences[7,41]. However, during bacterial chemotaxis in static gradients, the signal is generated from the cell's own motion.
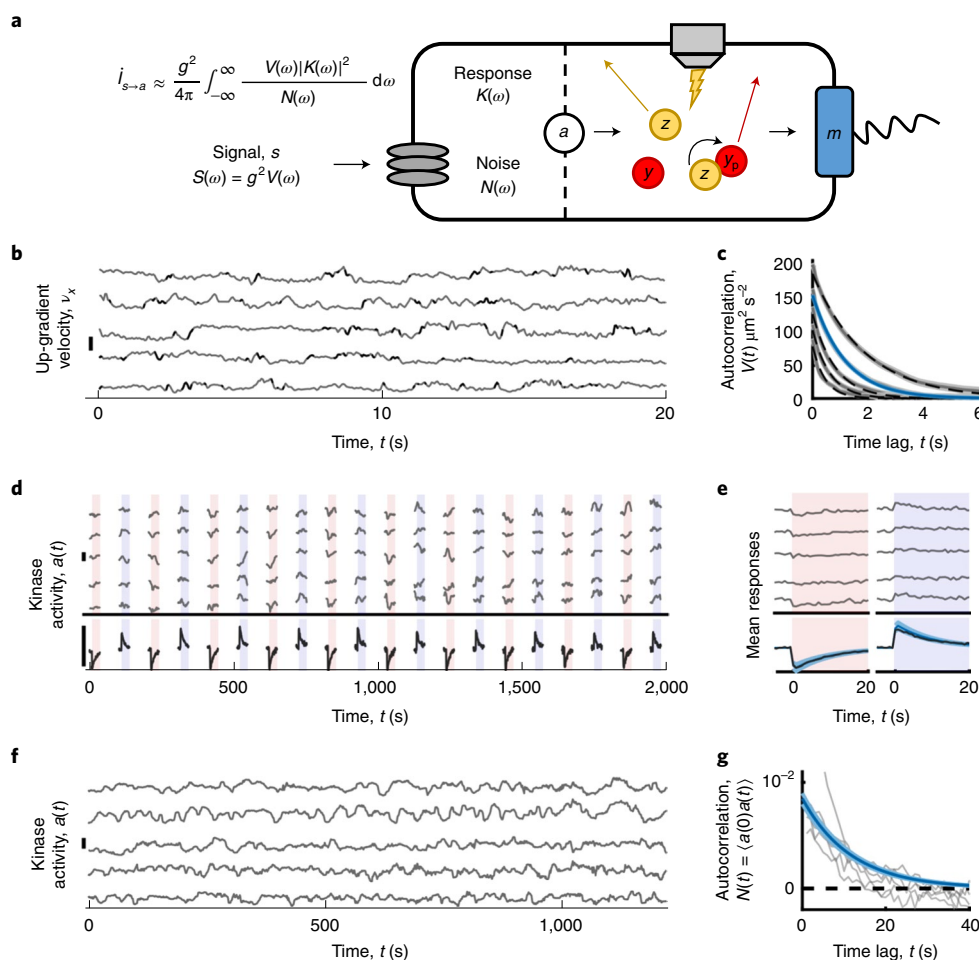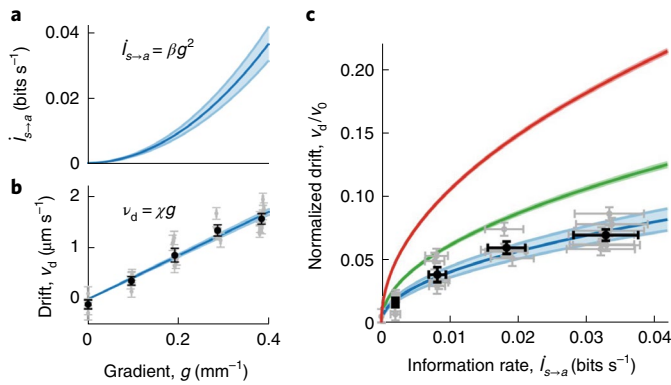
Fig. 2 | Measuring the rate of information transfer from signal to intracellular kinase. a, Information rate $\dot{I}_{s \rightarrow a}$ from signal s to kinase activity a depends on the signal power spectrum $S(\omega)$, kinase frequency response $K(\omega)$ and kinase noise power spectrum $N(\omega)$. The signal is $s(t) = g v_x(t)$, where g is the gradient steepness and v_x is the cell's up-gradient velocity. Thus, $S(\omega) = g^2 V(\omega)$, where $V(\omega)$ is the power spectrum of v_x. Kinase activity a was quantified from the FRET between the substrate of the kinase (CheY–mRFP, labelled y; the phosphorylated form is labelled y_p) and its phosphatase (CheZ–mYFP, labelled z) (Methods, Supplementary Sections 10–15 and Supplementary Figs. 3–6). All of the experiments were performed in a background of 100 μM methyl-aspartate (MeAsp). **b**, Grey, $v_x(t)$ of individual cells; black, tumbles; scale bar, 40 μm s^{-1}. **c**, Grey, average autocorrelation of v_x, $V(t)$, for $P_{run} = 0.93$, 0.89, 0.84, 0.79 and 0.74 (top to bottom; shading is ±1 s.e. black dashed lines are fits to $V(t) = a_v \exp(-\lambda_{tot}|t|)$. Blue, best fit to the median bin, namely, $P_{run} \approx 0.89$ (Supplementary Fig. 2 and Supplementary Section 21). **d**, Immobilized cells were delivered 10 μM step changes of MeAsp concentration, up (red shading) and down (blue shading). Top: grey, $a(t)$ for five cells (here and in **f**, smoothed with a tenth-order median filter; scale bars, $\Delta a = 0.3$; additional information in Methods, Supplementary Section 16 and Supplementary Fig. 5). Bottom: black, population average $a(t)$ ($n = 442$ cells). **e**, Single-cell average (top, grey) and population-average (bottom, black) responses to positive and negative stimuli. Blue line, $K(t) = G \exp(-t/\tau_2)(1 - \exp(-t/\tau_1)) H(t)$, where $H(t)$ is the Heaviside step function and G, τ_1 and τ_2 are the median parameters extracted from fits to single-cell responses. **f,g**, Grey, kinase activity (**f**) and corresponding autocorrelations (**g**) in single cells (Methods, Supplementary Section 17 and Supplementary Fig. 6). The blue line in **g** shows $N(t) = \langle a(t) a(0) \rangle = \sigma_n^2 \exp(-|t|/\tau_n)$, where σ_n and τ_n are the median parameters extracted from fits to single-cell traces ($n = 262$ cells). Also, $V(\omega)$, $K(\omega)$ and $N(\omega)$ are shown in Supplementary Fig. 7.

Thus, the signal power spectrum is $S(\omega) = g^2 V(\omega)$, where $V(\omega)$ is the power spectrum of the cell's up-gradient velocity $v_x(t)$. Furthermore, in shallow gradients, the statistics of $v_x(t)$ are nearly identical to those in the absence of a gradient (Supplementary Sections 8 and 9). To quantify the autocorrelation function of v_x ($V(t)$, and thus $V(\omega)$), we tracked individual swimming cells in a 100 μM background of the attractant α-methyl-aspartate (MeAsp) (Fig. 2b,c, Supplementary Fig. 2, Methods and Supplementary Sections 18–21). For each value of P_{run}, we fit the measured $V(t)$ with a decaying exponential, namely, $V(t) = a_v e^{-\lambda_{tot}|t|}$, giving $a_v = 157.1 \pm 0.5$ μm^2 s^{-2} and $\lambda_{tot} = 0.862 \pm 0.005$ s^{-1} for the median phenotype (total trajectory time, ~10^4 s; average duration, 7 s; Supplementary Table 1).

Next, we measured the response and noise properties of CheA kinase activity using Förster resonance energy transfer (FRET)

between the kinase's substrate CheY and the phosphatase CheZ inside single cells[17,18,42] (Fig. 2a). In the linear regime, the kinase response is characterized by its frequency-response function, $K(\omega)$, or its response $K(t)$ to an impulse of signal ($s(t) = \frac{d}{dt} \log(c)$). To measure $K(t)$, we used a microfluidic device that can rapidly switch (within ~100 ms) the attractant concentration delivered to hundreds of immobilized cells[42] (Supplementary Figs. 3 and 4). To ensure that the cells were in the log-sensing regime[12,43], we first adapted them to a background of 100 μM MeAsp. We then delivered 10 positive and 10 negative 10% step changes of MeAsp concentration (impulses of s) (Fig. 2d and Methods), which were small enough to be in the linear-response regime[44,45] (Supplementary Fig. 5). Cell responses exhibited a stereotypical shape (Fig. 2e) described by a phenomenological model $K(t) = G e^{-t/\tau_2}(1 - e^{-t/\tau_1}) H(t)$, with gain G,

Fig. 3 | *E. coli* cells efficiently use information to navigate. a, The rate of information transfer from signal to kinase activity depends on the gradient steepness g, that is, $\dot{I}_{s\to a}=\beta g^2$ ($\beta=0.22\pm0.03$ bits s^{-1} mm^2; Fig. 2 and Supplementary Section 8). In all panels, the shading and error bars indicate ±1 s.e. **b**, Chemotactic performance v_d as a function of gradient steepness g, in a background of 100 μM MeAsp. Grey dots, average drift speeds in individual experiments. Black dots, averages over experiments. Error bars on g are smaller than the markers. Population-average drift speed increases linearly with the gradient steepness, $v_d=\chi g$ ($\chi=4,300\pm150$ μm^2 s^{-1}; blue line and shading; Supplementary Section 22). **c**, From measurements of *E. coli* cells' information rates and chemotactic drift speeds, we compared their performance with the theoretical bound (equation (1)). Green, predicted maximum performance given the information-acquisition rate $\dot{I}_{s\to a}$ (equation (1)), with measured behavioural parameters $\theta=\{\lambda_{R0}, P_{run}, \alpha\}$ ($f(\theta)=0.531\pm0.005$). Blue, measured performance v_d/v_0 ($v_0=22.61\pm0.07$ μm s^{-1}) versus information rate $\dot{I}_{s\to a}$, obtained by eliminating g from the fits of $v_d(g)=\chi g$ and $\dot{I}_{s\to a}(g)=\beta g^2$ to plot $v_d/v_0=\chi/v_0\left(\dot{I}_{s\to a}/\beta\right)^{1/2}$. Black and grey dots are data points from **b** plotted against $\dot{I}_{s\to a}(g)=\beta g^2$. Taking the ratio of the blue and green curves, we find that *E. coli* cells achieve drift speeds within a factor $\eta=0.65\pm0.05$ of the theoretical limit. Red, theoretical bound (equation (1)) if λ_{R0} is optimized, and all the other behavioural parameters are held fixed at their measured values ($f(\theta)=0.914\pm0.006$, just below the maximum value of 1).

rise time τ_1, adaptation time τ_2 and Heaviside step function $H(t)$. We simultaneously fit this model to each cell's responses to the positive and negative stimuli (Supplementary Section 16) and then determined the population-median parameter values ($n=442$ cells) (Supplementary Table 1 and Supplementary Fig. 5): $G=1.73\pm0.03$, $\tau_1=0.22\pm0.01$ s, and $\tau_2=9.90\pm0.30$ s. This value of τ_1 includes the stimulus-switching time and CheY/CheZ-binding kinetics, making it longer than the kinase response time, which was previously measured to be $\tau_1\approx1/60$ s (refs. [46,47]). After verifying that our results are insensitive to the value of τ_1 (Supplementary Section 9 and Supplementary Fig. 8), we used the literature value in our estimate of $\dot{I}_{s\to a}$.

We quantified the statistics of noise in the kinase activity by measuring FRET in single cells in a constant background of 100 μM MeAsp (Fig. 2f and Supplementary Fig. 6). These fluctuations were well approximated by an Ornstein–Uhlenbeck process, consistent with previous measurements[16,18]. Using Bayesian filtering (Supplementary Section 17), we directly inferred the single-cell parameters of the noise model from the time series. These parameters determined the noise autocorrelation function $N(t)=\sigma_n^2 e^{-|t|/\tau_n}$ (Fig. 2g and Supplementary Section 9) and power spectrum $N(\omega)$ (Supplementary Fig. 7). The population-median parameter values ($n=262$ cells) were $\sigma_n=0.092\pm0.002$ arb. units (standard deviation of noise) and $\tau_n=11.75\pm0.04$ s (noise correlation time) (Supplementary Table 1). These measurements include the effects of all the noise sources upstream of CheA, including stochastic ligand arrivals at the cells' receptors[15].

With the signal statistics, response function and noise, we then computed the information rate from the signal to kinase activity $\dot{I}_{s\to a}$ (Fig. 3a). Since the signal power is proportional to g^2, so is the information rate: $\dot{I}_{s\to a}=\beta g^2$. Using our measurements above, we estimated that the *E. coli* chemotaxis system transfers information to the kinases at a rate of $\beta=0.22\pm0.03$ bits s^{-1} mm^2 (Supplementary Sections 8 and 9). Thus, in shallow gradients, where concentration varies on length scales of millimetres to centimetres, cells only get $\sim10^{-2}$ bits s^{-1}. The bound in equation (1) predicts that this is sufficient for a run-and-tumble navigator to climb gradients at a few percent of its swimming speed. However, it is unclear how much of this information is relevant to chemotaxis, communicated to the motors, and used to navigate.

To answer this, we measured *E. coli*'s average drift speeds by tracking individual cells' motion in gradients of varying steepness. Static, linear MeAsp gradients were constructed (Methods) in a 100 μM background, with length scales ranging from 10.0 mm ($g=0.1$ mm^{-1}) to 2.5 mm ($g=0.4$ mm^{-1}). From $>10^5$ s of trajectories in each condition, we estimated the drift speed v_d as the time-averaged up-gradient velocity over all the cells in each experiment (Supplementary Section 22). As expected from theory in shallow gradients, the drift speed increased linearly with gradient steepness $v_d=\chi g$, with 'chemotactic coefficient' $\chi\approx4.30\pm0.15$ μm s^{-1} mm^1 (Fig. 3b and Supplementary Fig. 9), consistent with previous measurements[48].

With measurements of both information-acquisition rate and performance, we were in a position to quantify how efficiently *E. coli* use information, η. For each gradient g, we plotted the drift speed $v_d(g)$ against the information rate $\dot{I}_{s\to a}(g)$ (Fig. 3c, blue). On the same plot, we show the maximum drift speeds, given by the bound in equation (1) (Fig. 3c, green). The ratio of these two curves is the efficiency $\eta=\chi/\left[v_0 f(\theta)\left(\dfrac{\log(2)\,\beta}{12\,D_r}\right)^{1/2}\right]$, which is independent of g in shallow gradients. We find that *E. coli* cells achieve an efficiency of $\eta=0.65\pm0.05$—that is, they climb gradients at $\sim65\%$ of the maximum possible speed given the rate at which their kinases encode information about environmental signals. Equivalently, comparing information rates (Fig. 3c, blue and green lines) at the same drift speed indicates that $\eta^2=\dot{I}^*_{s\to m}/\dot{I}_{s\to a}\approx42\%$ of the total information available in kinase activity is relevant, preserved in communication with the motors, and used to navigate.

Many studies of information theory in biology have focused on the maximum amount of information that signalling pathways can transmit[1–6,49–51]. Instead, here we asked how the information an organism transmits limits its performance at functional tasks, using *E. coli* chemotaxis as the model system. Although previous works measured one-shot information transfer by biochemical networks[1–6,49–51] (measured in bits), we measured the rate at which *E. coli* cells continuously transfer information (measured in bits s^{-1}) between time-varying inputs and outputs, with natural input statistics. Combining this with measurements of *E. coli*'s chemotactic performance and the theoretical limit (equation (1)), we found that about half the information about concentration changes that flows through CheA is both relevant to and used for navigation.

Achieving high efficiency requires that cells acquire, transmit and act on the information that is relevant to their task[10], but which bits are relevant is often not clear. Using rate-distortion theory[6,52,53], we found that the relevant bits for bacterial chemotaxis are those that indicate how fast the attractant concentration is currently changing (Supplementary Section 5). Responding to signals that the cell experienced multiple signal correlation times τ_ν in the past results in the transmission of a substantial amount of irrelevant information, where $\tau_\nu^{-1}=(1-\alpha)\lambda_{R0}+2D_r$ (Supplementary Section 5). However, in typical gradients, which are much longer than their body lengths, *E. coli* cells must swim and time integrate to infer signals from stochastic ligand arrivals[15,54]. This forces *E. coli* cells to respond to past signals to learn about the current signal, thus transmitting irrelevant

information and preventing them from reaching the bound in equation (1). Between the green and blue lines (Fig. 3c), there is a tighter bound on performance that accounts for the need to time integrate, relative to which *E. coli* cells are even more efficient.

The information-performance bound in equation (1) depends on the cell's swimming behaviour. We quantified this bound for a typical cell from a laboratory strain, but behavioural parameters θ vary across individual cells[16,36–39,55], strains and growth conditions[56]. This raises the question of what behavioural phenotype can achieve the highest performance with a given information rate. Maximizing $f(\theta)$ with respect to θ (Supplementary Section 6), we find that the optimal agent changes direction by tumbling at the same rate as rotational diffusion[33,57,58], that is, $(1 - \alpha)\lambda_{R0} = 2D_r$. Our median phenotype tumbles more frequently than this and misses out twofold. First, the bound on its performance (Fig. 3c, green) is about half as high as it could be (Fig. 3c, red). Second, a lower average tumble rate λ_{R0} would lengthen the signal correlation time τ_v, increasing the fraction of relevant information that the cell would transfer and thus increasing η relative to the higher bound. Laboratory strains of *E. coli* were historically selected for motility in semisolid agar[59–61], and our strain's frequent reorientations may be optimized to navigate that environment[62–64]. Alternatively, their behavioural parameters may optimize other objectives[31,33]. Although *E. coli*'s behavioural strategy thus appears sub-optimal for gradient climbing in a liquid, the cells nevertheless efficiently use biochemical information in CheA to carry it out.

A hallmark of *E. coli*'s chemotactic response to many ligands—including MeAsp used here—is precise adaptation[65]: following a stimulus, the kinase activity transiently responds before relaxing back to the pre-stimulus activity (Fig. 2e). However, for some attractants, such as serine, adaptation is imperfect, causing the average tumble rate to decrease with increasing concentration of attractant in the background[30,37,57,66–68]. By lowering λ_{R0} closer to the optimal value, a background of serine both increases the bound and causes cells to climb gradients of MeAsp faster[67] (Supplementary Section 7). However, from an information-usage perspective, if the cell could independently choose λ_{R0} and its response function, our theory shows that it should match its average tumble rate to the rotational diffusion coefficient, that is, $(1 - \alpha)\lambda_0 = 2D_r$, and its response function should adapt perfectly. Imperfect adaptation implies that the cell is responding to concentration changes that occurred far in the past, which transfers irrelevant information.

Because we measured signal statistics and kinase activity in different cells, our estimate of the information rate does not account for the long tail in the run-length distribution that can arise from fluctuations in kinase activity[16,69–71]. In theory, these fluctuations can improve the performance in shallow gradients[72,73]. However, they only contribute corrections to the information rate that are of a higher order in g and can be neglected in shallow gradients (Supplementary Section 8).

This work relied on linear theory, which is only valid in shallow gradients. In steep gradients, behavioural feedback can drive large deviations in the tumble rate, leading to ratchet-like gradient climbing[25]. In this regime, the signal statistics gain multiple time scales due to the very different run durations up and down the gradient. In future studies, it will be interesting to examine how these factors—combined with nonlinearities in the signalling pathway—alter cells' information-acquisition rates and efficiencies.

Here we measured information transfer at two very different length scales. The first is the relevant information contained in the behaviour, which is quantified by the drift speed and behavioural parameters. The second is the total information available in the CheA kinase activity. Considering how different these measurements are, there is no reason to expect that they must be similar in magnitude. However, their agreement within about a factor of two is a strong indication that information is a limitation on chemotaxis

performance. Information transfer is not necessarily the end goal of biological tasks, but it is needed to perform many of them. Our results suggest organisms may be under selective pressure to efficiently use information from environmental cues to perform tasks necessary for their survival.

Online content

References

1. Cheong, R., Rhee, A., Wang, C. J., Nemenman, I. & Levchenko, A. Information transduction capacity of noisy biochemical signaling networks. *Science* **334**, 354–358 (2011).
2. Uda, S. et al. Robustness and compensation of information transmission of signaling pathways. *Science* **341**, 558–561 (2013).
3. Selimkhanov, J. et al. Accurate information transmission through dynamic biochemical signaling networks. *Science* **346**, 1370–1373 (2014).
4. Granados, A. A. et al. Distributed and dynamic intracellular organization of extracellular information. *Proc. Natl Acad. Sci. USA* **115**, 6088–6093 (2018).
5. Bowsher, C. G. & Swain, P. S. Environmental sensing, information transfer, and cellular decision-making. *Curr. Opin. Biotechnol.* **28**, 149–155 (2014).
6. Tkačik, G. & Bialek, W. Information processing in living systems. *Annu. Rev. Condens. Matter Phys.* **7**, 89–117 (2016).
7. Laughlin, S. A simple coding procedure enhances a neuron's information capacity. *Z. Naturforsch. C J. Biosci.* **36**, 910–912 (1981).
8. Rieke, F., Warland, D. & Bialek, W. Coding efficiency and information rates in sensory neurons. *Europhys. Lett.* **22**, 151–156 (1993).
9. Petkova, M. D., Tkačik, G., Bialek, W., Wieschaus, E. F. & Gregor, T. Optimal decoding of cellular identities in a genetic network. *Cell* **176**, 844–855.e15 (2019).
10. Bialek, W., De Ruyter Van Stevenink, R. R. & Tishby, N. Efficient representation as a design principle for neural coding and computation. In *2006 IEEE International Symposium on Information Theory* 659–663 (IEEE, 2006).
11. Berg, H. C. *E. coli in Motion* (Springer, 2004).
12. Lazova, M. D., Ahmed, T., Bellomo, D., Stocker, R. & Shimizu, T. S. Response rescaling in bacterial chemotaxis. *Proc. Natl Acad. Sci. USA* **108**, 13870–13875 (2011).
13. Tu, Y. Quantitative modeling of bacterial chemotaxis: signal amplification and accurate adaptation. *Annu. Rev. Biophys.* **42**, 337–359 (2013).
14. Parkinson, J. S., Hazelbauer, G. L. & Falke, J. J. Signaling and sensory adaptation in *Escherichia coli* chemoreceptors: 2015 update. *Trends Microbiol.* **23**, 257–266 (2015).
15. Berg, H. C. & Purcell, E. M. Physics of chemoreception. *Biophys. J.* **20**, 193–219 (1977).
16. Korobkova, E., Emonet, T., Vilar, J. M. G., Shimizu, T. S. & Cluzel, P. From molecular noise to behavioural variability in a single bacterium. *Nature* **428**, 574–578 (2004).
17. Colin, R., Rosazza, C., Vaknin, A. & Sourjik, V. Multiple sources of slow activity fluctuations in a bacterial chemosensory network. *eLife* **6**, e26796 (2017).
18. Keegstra, J. M. et al. Phenotypic diversity and temporal variability in a bacterial signaling network revealed by single-cell FRET. *eLife* **6**, e27455 (2017).
19. Lan, G., Sartori, P., Neumann, S., Sourjik, V. & Tu, Y. The energy–speed–accuracy trade-off in sensory adaptation. *Nat. Phys.* **8**, 422–428 (2012).
20. Clausznitzer, D., Micali, G., Neumann, S., Sourjik, V. & Endres, R. G. Predicting chemical environments of bacteria from receptor signaling. *PLoS Comput. Biol.* **10**, e1003870 (2014).
21. Ito, S. & Sagawa, T. Maxwell's demon in biochemical signal transduction with feedback loop. *Nat. Commun.* **6**, 7498 (2015).
22. Micali, G. & Endres, R. G. Maximal information transmission is compatible with ultrasensitive biological pathways. *Sci. Rep.* **9**, 16898 (2019).
23. Shannon, C. E. A mathematical theory of communication. *Bell Syst. Tech. J.* **27**, 379–423 (1948).
24. Tostevin, F. & ten Wolde, P. R. Mutual information between input and output trajectories of biochemical networks. *Phys. Rev. Lett.* **102**, 218101 (2009).
25. Long, J., Zucker, S. W. & Emonet, T. Feedback between motion and sensation provides nonlinear boost in run-and-tumble navigation. *PLoS Comput. Biol.* **13**, e1005429 (2017).

26. Hartich, D., Barato, A. C. & Seifert, U. Stochastic thermodynamics of bipartite systems: transfer entropy inequalities and a Maxwell's demon interpretation. *J. Stat. Mech.* **2014**, P02016 (2014).

27. Meijers, M., Ito, S. & ten Wolde, P. R. Behavior of information flow near criticality. *Phys. Rev. E* **103**, L010102 (2021).

28. Schreiber, T. Measuring information transfer. *Phys. Rev. Lett.* **85**, 461–464 (2000).

29. Sigtermans, D. Towards a framework for observational causality from time series: when Shannon meets Turing. *Entropy* **22**, 426 (2020).

30. de Gennes, P.-G. Chemotaxis: the role of internal delays. *Eur. Biophys. J.* **33**, 691–693 (2004).

31. Clark, D. A. & Grant, L. C. The bacterial chemotactic response reflects a compromise between transient and steady-state behavior. *Proc. Natl Acad. Sci. USA* **102**, 9150–9155 (2005).

32. Locsei, J. T. Persistence of direction increases the drift velocity of run and tumble chemotaxis. *J. Math. Biol.* **55**, 41–60 (2007).

33. Celani, A. & Vergassola, M. Bacterial strategies for chemotaxis response. *Proc. Natl Acad. Sci. USA* **107**, 1391–1396 (2010).

34. Becker, N. B., Mugler, A. & ten Wolde, P. R. Optimal prediction by cellular signaling networks. *Phys. Rev. Lett.* **115**, 258103 (2015).

35. Nakamura, K. & Kobayashi, T. J. Connection between the bacterial chemotactic network and optimal filtering. *Phys. Rev. Lett.* **126**, 128102 (2021).

36. Spudich, J. L. & Koshland, D. E. Non-genetic individuality: chance in the single cell. *Nature* **262**, 467–471 (1976).

37. Masson, J.-B., Voisinne, G., Wong-Ng, J., Celani, A. & Vergassola, M. Noninvasive inference of the molecular chemotactic response using bacterial trajectories. *Proc. Natl Acad. Sci. USA* **109**, 1802–1807 (2012).

38. Waite, A. J., Frankel, N. W. & Emonet, T. Behavioral variability and phenotypic diversity in bacterial chemotaxis. *Annu. Rev. Biophys.* **47**, 595–616 (2018).

39. Moore, J. P., Kamino, K. & Emonet, T. Non-genetic diversity in chemosensing and chemotactic behavior. *Int. J. Mol. Sci.* **22**, 6960 (2021).

40. Shannon, C. E. Communication in the presence of noise. *Proc. IRE* **37**, 10–21 (1949).

41. Rieke, F., Bodnar, D. A. & Bialek, W. Naturalistic stimuli increase the rate and efficiency of information transmission by primary auditory afferents. *Proc. R. Soc. Lond. B* **262**, 259–265 (1995).

42. Kamino, K., Keegstra, J. M., Long, J., Emonet, T. & Shimizu, T. S. Adaptive tuning of cell sensory diversity without changes in gene expression. *Sci. Adv.* **6**, eabc1087 (2020).

43. Kalinin, Y. V., Jiang, L., Tu, Y. & Wu, M. Logarithmic sensing in *Escherichia coli* bacterial chemotaxis. *Biophys. J.* **96**, 2439–2448 (2009).

44. Sourjik, V. & Berg, H. C. Receptor sensitivity in bacterial chemotaxis. *Proc. Natl Acad. Sci. USA* **99**, 123–127 (2002).

45. Shimizu, T. S., Tu, Y. & Berg, H. C. A modular gradient-sensing network for chemotaxis in *Escherichia coli* revealed by responses to time-varying stimuli. *Mol. Syst. Biol.* **6**, 382 (2010).

46. Francis, N. R. et al. Subunit organization in a soluble complex of Tar, CheW, and CheA by electron microscopy. *J. Biol. Chem.* **277**, 36755–36759 (2002).

47. Levit, M. N., Grebe, T. W. & Stock, J. B. Organization of the receptor-kinase signaling array that regulates *Escherichia coli* chemotaxis. *J. Biol. Chem.* **277**, 36748–36754 (2002).

48. Colin, R., Zhang, R. & Wilson, L. G. Fast, high-throughput measurement of collective behaviour in a bacterial population. *J. R. Soc. Interface* **11**, 20140486 (2014).

49. Potter, G. D., Byrd, T. A., Mugler, A. & Sun, B. Dynamic sampling and information encoding in biochemical networks. *Biophys. J.* **112**, 795–804 (2017).

50. Anders, A., Ghosh, B., Glatter, T. & Sourjik, V. Design of a MAPK signalling cascade balances energetic cost versus accuracy of information transmission. *Nat. Commun.* **11**, 3494 (2020).

51. Razo-Mejia, M. et al. First-principles prediction of the information processing capacity of a simple genetic circuit. *Phys. Rev. E* **102**, 022404 (2020).

52. Shannon, C. E. Coding theorems for a discrete source with a fidelity criterion. *IRE Nat. Conv. Rec.* **7**, 142–163 (1959).

53. Andrews, B. W. & Iglesias, P. A. An information-theoretic characterization of the optimal gradient sensing response of cells. *PLoS Comput. Biol.* **3**, e153 (2007).

54. Mora, T. & Wingreen, N. S. Limits of sensing temporal concentration changes by single cells. *Phys. Rev. Lett.* **104**, 248101 (2010).

55. Waite, A. J. et al. Non-genetic diversity modulates population performance. *Mol. Syst. Biol.* **12**, 895 (2016).

56. Ni, B., Colin, R., Link, H., Endres, R. G. & Sourjik, V. Growth-rate dependent resource investment in bacterial motile behavior quantitatively follows potential benefit of chemotaxis. *Proc. Natl Acad. Sci. USA* **117**, 595–601 (2020).

57. Berg, H. C. & Brown, D. A. Chemotaxis in *Escherichia coli* analysed by three-dimensional tracking. *Nature* **239**, 500–504 (1972).

58. Dufour, Y. S., Fu, X., Hernandez-Nunez, L. & Emonet, T. Limits of feedback control in bacterial chemotaxis. *PLoS Comput. Biol.* **10**, e1003694 (2014).

59. Armstrong, J. B., Adler, J. & Dahl, M. M. Nonchemotactic mutants of *Escherichia coli*. *J. Bacteriol.* **93**, 390–398 (1967).

60. Bachmann, B. J. Pedigrees of some mutant strains of *Escherichia coli* K-12. *Bacteriol. Rev.* **36**, 525–557 (1972).

61. Barker, C. S., Prüß, B. M. & Matsumura, P. Increased motility of *Escherichia coli* by insertion sequence element integration into the regulatory region of the *flhD* operon. *J. Bacteriol.* **186**, 7529–7537 (2004).

62. Wolfe, A. J. & Berg, H. C. Migration of bacteria in semisolid agar. *Proc. Natl Acad. Sci. USA* **86**, 6973–6977 (1989).

63. Licata, N. A., Mohari, B., Fuqua, C. & Setayeshgar, S. Diffusion of bacterial cells in porous media. *Biophys. J.* **110**, 247–257 (2016).

64. Kurzthaler, C. et al. A geometric criterion for the optimal spreading of active polymers in porous media. Preprint at https://arxiv.org/abs/2106.05366 (2021).

65. Alon, U., Surette, M. G., Barkai, N. & Leibler, S. Robustness in bacterial chemotaxis. *Nature* **397**, 168–171 (1999).

66. Neumann, S., Vladimirov, N., Krembel, A. K., Wingreen, N. S. & Sourjik, V. Imprecision of adaptation in *Escherichia coli* chemotaxis. *PLoS ONE* **9**, e84904 (2014).

67. Wong-Ng, J., Melbinger, A., Celani, A. & Vergassola, M. The role of adaptation in bacterial speed races. *PLoS Comput. Biol.* **12**, e1004974 (2016).

68. Wong-Ng, J., Celani, A. & Vergassola, M. Exploring the function of bacterial chemotaxis. *Curr. Opin. Microbiol.* **45**, 16–21 (2018).

69. Tu, Y. & Grinstein, G. How white noise generates power-law switching in bacterial flagellar motors. *Phys. Rev. Lett.* **94**, 208101 (2005).

70. Park, H., Oikonomou, P., Guet, C. C. & Cluzel, P. Noise underlies switching behavior of the bacterial flagellum. *Biophys. J.* **101**, 2336–2340 (2011).

71. Huo, H., He, R., Zhang, R. & Yuan, J. Swimming *Escherichia coli* cells explore the environment by Lévy walk. *Appl. Environ. Microbiol.* **87**, e02429-20 (2021).

72. Flores, M., Shimizu, T. S., ten Wolde, P. R. & Tostevin, F. Signaling noise enhances chemotactic drift of *E. coli*. *Phys. Rev. Lett.* **109**, 148101 (2012).

73. Sneddon, M. W., Pontius, W. & Emonet, T. Stochastic coordination of multiple actuators reduces latency and improves chemotactic response in bacteria. *Proc. Natl Acad. Sci. USA* **109**, 805–810 (2012).

Methods

Strains and plasmids. The strain used for the FRET experiments is a derivative of the *E. coli* K-12 strain RP437 (HCB33), a gift from T. Shimizu, and described in detail elsewhere[18,42]. In brief, the FRET acceptor–donor pair (CheY–mRFP and CheZ–mYFP) is expressed in tandem from plasmid pSJAB106 (ref. [18]) under an isopropyl β-D-thiogalactopyranoside (IPTG)-inducible promoter. The glass-adhesive mutant of FliC (FliC*) was expressed from a sodium salicylate (NaSal)-inducible pZR1 plasmid[18]. The plasmids are transformed in VS115, a *cheY cheZ fliC* mutant of RP437 (ref. [18]) (gift from V. Sourjik). The cross-talk coefficient for spectral bleedthrough was measured using a strain expressing CheZ–YFP from a plasmid, and that for cross-excitation was measured using a strain expressing CheY–mRFP from a plasmid, both of which are gifts from T. Shimizu. RP437, the direct parent of the FRET strain and also a gift from T. Shimizu, was used to measure the behavioural parameters and chemotactic drift speeds. A mutant that cannot tumble due to an in-frame deletion of the *cheY* gene, namely, VS100 (gift from V. Sourjik), was used to measure the rotational diffusion coefficient D_r. All the strains are available from the authors on request.

Cell preparation. Single-cell FRET microscopy and cell culture were carried out essentially as described previously[18,42]. In brief, cells were picked from a frozen stock at −80 °C and inoculated in 2 ml tryptone broth (TB; 1% bacto-tryptone, 0.5% NaCl) and grown overnight to saturation at 30 °C and shaken at 250 r.p.m. Cells from the saturated overnight culture were diluted 1 part in 100 in 10 ml TB and grown to an optical density value of 0.45–0.47 at 600 nm (OD600) in the presence of 100 μg ml⁻¹ ampicillin, 34 μg ml⁻¹ chloramphenicol, 50 μM IPTG and 3 μM NaSal at 33.5 °C and shaking at 250 r.p.m. Cells were collected by centrifugation (5 min at 5,000 r.p.m. or 4,080 relative centrifugal force (RCF)) and washed twice with a motility buffer (10 mM KPO₄, 0.1 mM EDTA, 1 μM methionine and 10 mM lactic acid; pH 7), and then were resuspended in 2 ml motility buffer. Cells were left at 22 °C for 90 min before loading into the microfluidic device. All of the experiments involving FRET or swimming were performed at 22–23 °C.

For swimming and chemotaxis experiments, cells were identically prepared. Saturated overnight cultures were diluted 1 part in 100 in 5 ml TB. After growing to an OD600 value of 0.45–0.47, 1 ml cell suspension was washed twice in the motility buffer with 0.05% w/v of polyvinylpyrrolidone-40 (PVP-40; molecular weight (MW), 40 kDa). Washes were done by centrifuging the suspension in an Eppendorf tube at 1,700 RCF (4,000 r.p.m. in this centrifuge) for 3 min. After the last wash, the cells were resuspended with varying concentrations of MeAsp (see below).

Microfluidic device fabrication and loading for FRET measurements. Microfluidic devices for the FRET experiments[42] were constructed from polydimethylsiloxane (PDMS) on 24 × 60 mm² cover glasses (#1.5) following standard soft lithography protocols[74]. Briefly, the master moulds for the device were created with a negative SU-8 photoresist on 100 mm silicon wafers. Approximately 16-μm-high master moulds were created. To fabricate the device, the master moulds were coated with a 5-mm-thick layer of degassed 10:1 PDMS:curing agent mixture (Sylgard 184, Dow Corning). The PDMS layer was cured at 80 °C for 1 h, cut and separated from the wafer, and holes were punched for inlets and outlet. The punched PDMS layer was further cured at 80 °C for >2 h. Then, the PDMS layer was cleaned with a transparent adhesive tape (Magic Tape, Scotch) followed by rinsing with isopropanol, methanol and Millipore-filtered water, in that order. The glass was rinsed with acetone, isopropanol, methanol and Millipore-filtered water, in that order. The PDMS device was cleaned with the tape an additional time before the surfaces of the device and coverslip were treated in a plasma-bonding oven (Harrick Plasma). After 1 min of exposure to plasma under a vacuum, the device was laminated to the coverslip and then baked at 80 °C on a hot plate for >30 min to establish a covalent bond.

Sample preparation in the microfluidic device was conducted as follows. Five inlets of the device (Supplementary Fig. 3) were connected to reservoirs (C3669 liquid chromatography columns, Sigma-Aldrich) filled with motility buffer containing various concentrations of MeAsp via polyethylene tubing (polythene tubing; inner diameter, 0.58 mm; outer diameter, 0.96 mm; BD Intramedic). The tubing was connected to the PMDS device through stainless steel pins that were directly plugged into the inlets or outlet of the device (New England Tubing). Cells—washed and suspended in the motility buffer—were loaded into the device from the outlet and allowed to attach to the cover glass surface via their sticky flagella by reducing the flow speed inside the chamber. The pressure applied to the inlet solution in the reservoirs was controlled by computer-controlled solenoid valves (MH1, Festo), which rapidly switched between atmospheric pressure and higher pressure (1.0 kPa) using a source of pressurized air. Only one experiment was conducted per device.

Single-cell FRET imaging system. FRET imaging in the microfluidic device was performed using an inverted microscope (Eclipse Ti-E, Nikon) equipped with an oil-immersion objective lens (CFI Apo TIRF 60X Oil, Nikon). Yellow fluorescent protein (YFP) was illuminated by a light-emitting diode illumination system (SOLA SE, Lumencor) through an excitation bandpass filter (FF01-500/24-25, Semrock) and a dichroic mirror (F01-542/27-25F, Semrock). The

fluorescence emission was led into an emission image splitter (OptoSplit II, Cairn) and further split into donor and acceptor channels by a second dichroic mirror (FF580-FDi01-25×36, Semrock). The emission was then collected through emission bandpass filters (FF520-Di02-25×36 and FF593-Di03-25×36, Semrock) by a scientific complementary metal–oxide–semiconductor (sCMOS) camera (ORCA-Flash4.0 V2; Hamamatsu). Red fluorescent protein (RFP) was illuminated in the same way as YFP, except that an excitation bandpass filter (FF01-575/05-25, Semrock) and a dichroic mirror (FF593-Di03-25×36, Semrock) were used. An additional excitation filter (59026x, Chroma) was used in front of the excitation filters. To synchronize image acquisition and delivery of stimulus solutions, a custom-made MATLAB program was used to control both the imaging system (through the application programming interface provided by μManager[75]) and the states of the solenoid valves.

Procedure for measuring the linear-response functions. All the experiments were performed in a background MeAsp concentration of $c_0 = 100$ μM. Measurements were made in single cells. First, the FRET level at the minimum kinase activity was measured by delivering a saturating stimulus (1 mM MeAsp and 100 μM serine)[76] for 10 s. Immediately afterwards, the FRET level at the maximum kinase activity was measured by delivering motility buffer with no attractant (0 μM MeAsp and 0 μM serine) for 5 s. When the cells are adapted to 100 μM MeAsp, removing all of the attractants is sufficient to elicit the maximum response[18,44]. The donor was excited every 0.5 s (to measure the donor excitation–donor emission signal I_{DD} and the donor excitation–acceptor emission signal I_{DA}; see Supplementary Section 10) and the acceptor was excited before and after the set of donor excitations (to measure the acceptor excitation–acceptor emission signal I_{AA}). After this, the concentration of MeAsp was returned to the background c_0, and no serine was delivered to the cells for the rest of the experiment. Imaging was then stopped and the cells were allowed to adapt to the background for 120 s.

After this, a series of stimuli were delivered to the cells in the microfluidic device (Fig. 2e shows the stimulus protocol). Importantly, the cells were only illuminated and imaged for part of the experiment to limit photobleaching. First, cells were imaged for 7.5 s in the background concentration c_0. Then, the concentration of MeAsp was shifted up to $c_+ = 110$ μM for 30 s and the imaging was continued. The donor excitation interval was 0.75 s and acceptor excitations were done before and after the set of donor excitations. After this time, imaging was stopped and the MeAsp concentration was returned to c_0 for >60 s to allow the cells to adapt. Then, the same process was repeated, but this time, the MeAsp concentration was decreased to $c_- = 90$ μM. Alternating up and down stimuli were repeated 10 times each.

The change in concentration experienced by the cells in this experiment is much larger than the changes experienced by cells swimming in our gradient experiments. Ideally, we could deliver the same magnitude of stimulus to the cells under both conditions. However, to detect the responses to stimuli as small as the ones experienced in the gradient experiments above the noise in a FRET experiment, we would need to deliver and average over responses to many more instances of the stimulus. The photon budget is a major constraint when imaging in single cells, making this impossible. We chose the 10% stimuli to balance the need to measure responses above noise, in addition to keeping the response in the linear regime[44,45] (Supplementary Fig. 5).

FRET levels at the minimum and maximum kinase activity were measured again at the end of the experiment. The whole imaging protocol lasted <2,200 s. In total, the cells spent <60 min in the device, from loading to the end of imaging. Analyses of these data are described in Supplementary Sections 10–16.

Procedure for measuring the noise statistics. Spontaneous fluctuations in kinase activity were also measured in a background MeAsp concentration of $c_0 = 100$ μM. Measurements were made in single cells. FRET levels at the minimum and maximum kinase activity were measured at the beginning and end of each experiment, as described above. Similarly, after these measurements, imaging was stopped and cells were allowed to adapt to the background for 120 s. After this, cells were imaged for about 1,200 s. In these experiments, donor excitations (that is, measurements of I_{DD} and I_{DA}; Supplementary Information) were done every 1.0 s, except when it was interrupted by acceptor excitations (that is, measurements of I_{AA}; Supplementary Information), which were conducted every 100 donor excitations. The whole imaging protocol lasted <1,400 s. In total, the cells spent about <60 min in the device, from loading to the end of imaging. Analyses of these data are described in Supplementary Sections 10–15 and 17.

Procedure for measuring swimming and behavioural parameters. After the second wash, cells were centrifuged again and resuspended in the motility buffer containing 100 μM MeAsp. Then, the cell suspension was diluted to an OD600 value of 0.00025. The cell suspension was then loaded into μ-Slide Chemotaxis devices (ibidi)—the same type of device used to create static gradients, as described below. However, instead of tracking cells in the gradient region, we tracked their swimming pattern in one of the large reservoirs, which are roughly 750 μm deep. Here 1,000-s-long movies of swimming cells were recorded on a Nikon Ti-E inverted microscope using a CFI Plan Fluor 4X objective (numerical aperture (NA), 0.13). This objective's depth of field is about ±18 μm—much shorter than the depth

of the chamber. Adjusting the focal plane to the middle of the chamber made cells that were swimming near the ceiling or floor of the device, which could experience hydrodynamic interactions that affect their behaviour[77,78], not visible in the movie. At the same time, this lower-magnification objective allowed us to collect relatively longer swimming trajectories. Movies were captured around 30 min after loading cells into the chamber to mimic the gradient experiments below. Images here and below were captured using an sCMOS camera (ORCA-Flash4.0 V2, Hamamatsu). Analyses of these data are described in Supplementary Sections 18–21. Five biological replicates were obtained for behavioural parameter measurements, and four biological replicates were obtained to measure D_r.

Procedure for measuring chemotactic drift speeds. Chemotaxis experiments were performed in μ-Slide Chemotaxis devices (ibidi). These devices generate a linear gradient between two concentration reservoirs that is stable for a long time. After the second wash, the cell suspension was split into two Eppendorf tubes, 0.5 ml each. After one more centrifugation, one tube of cells was resuspended in 1 ml motility buffer with 100 μM MeAsp, to be injected into the 'low-concentration reservoir', and the other was resuspended in 1 ml motility buffer with 2 μM fluorescein and varying concentrations of attractant, to be injected into the 'high-concentration reservoir'. Cells in both tubes were diluted to an optical density value of 0.001 for each experiment. Loading cells in both reservoirs ensured that the concentration of cells throughout the experimental device was approximately uniform. This limited the effects of potential biases that could arise from observing a finite field of view.

Using a background concentration of at least 100 μM MeAsp ensured that the cells were in the log-sensing regime[12]. The 'high' concentrations of MeAsp used were 110.5, 122.1, 135.0 and 149.2 μM. With 1 mm separating the two reservoirs, these concentrations produced linear gradients that approximated shallow exponential gradients with steepness of roughly $g = \{0.1, 0.2, 0.3, 0.4\}$ mm^{-1}. Here g was calculated using $g = \frac{\Delta \log c}{\Delta x}$, where $\Delta\log(c)$ is the difference in log concentrations between the two reservoirs and Δx is the distance between them. This is exactly the average steepness of log concentration across the width of the channel. To see this, the steady-state concentration profile is linear, $c(x) = \frac{\Delta c}{\Delta x}(x - x_0) + c_0$, where Δc is the difference in concentrations between the two reservoirs, x_0 is the midpoint between them and c_0 is the concentration at $x = x_0$. From this, the gradient of log concentration depends on position x and can be computed using $g(x) = \frac{d\log(c(x))}{dx} = \frac{1}{\frac{1}{c_0}\frac{\Delta c}{\Delta x}x+1}\frac{1}{c_0}\frac{\Delta c}{\Delta x}$, where we have defined a reference frame for which $x_0 = 0$. Averaging over the channel by integrating over x from $-\Delta x/2$ to $\Delta x/2$ and dividing by Δx gives $g = \frac{\log\left(1 + \frac{1}{2}\frac{\Delta c}{c_0}\right) - \log\left(1 - \frac{1}{2}\frac{\Delta c}{c_0}\right)}{\Delta x} = \frac{\log\left(c_0 + \frac{1}{2}\Delta c\right) - \log\left(c_0 - \frac{1}{2}\Delta c\right)}{\Delta x} = \frac{\Delta\log c}{\Delta x} = g$. Close to the low-concentration reservoir, $g(x)$ is larger than g, and vice versa near the high-concentration reservoir, but these errors are small and approximately cancel each other out when we average drift speeds of cells across the channel.

To load the device, first, the reservoirs were sealed with the manufacturer's tabs. Cell suspension with 100 μM MeAsp was injected into the channel where the gradient would form. Excess liquid in the inlets was removed. Then, one tab from each reservoir was removed, and the gradient channel was sealed with tabs. The left reservoir was then fully unsealed, and the right reservoir was sealed with tabs. Here 60–65 μl cell suspension with 100 μM MeAsp was injected into the left reservoir, and then both inlets of that reservoir were sealed with tape or tabs. Care was taken to make sure there were no bubbles in the reservoir at the inlets. Then, the right reservoir was unsealed, and 60–65 μl cell suspension with the higher concentration of MeAsp was injected. A timer was then immediately started. The right reservoir was then sealed.

Cells were imaged using phase contrast with a CFI Plan Fluor 10X objective (NA, 0.30). The depth of the gradient region of the device is 70 μm, and the depth of field of the objective is about ±4 μm. Focusing on the middle of the chamber with this objective filtered out the cells that could be interacting with the ceiling or floor surfaces. Images of fluorescein were taken every 5 min using a CFI Plan Fluor 4X objective (NA, 0.13) through a YFP filter cube (49003, Chroma), illuminated by a light-emitting diode (SOLA SE, Lumencor) with an exposure time of 100 ms. Since the diffusivity of fluorescein is similar to (slightly lower than) that of MeAsp (MW of fluorescein, 376 kDa, and MW of MeAsp, 147 kDa; Sigma-Aldrich), we used fluorescein as an indication of when the attractant gradient was stable and linear in the observation region between the two reservoirs, as done before[48,55]. Once the fluorescein profile was stable for several time points (typically around 50–60 min after loading), a 1,000-s-long phase-contrast movie was recorded at 20 frames per second using the 10X phase-contrast objective. Before the recording,

the transmitted light illumination was adjusted to minimize the number of saturated pixels. After the recording, an additional image of the fluorescein profile was recorded, and the cells were observed to check that they were still swimming normally. Analyses of these data are described in Supplementary Section 21. At least five biological replicates were performed for each gradient steepness.

Reporting Summary. Further information on research design is available in the Nature Research Reporting Summary linked to this article.

Data availability
Source data are provided with this paper. Source data for the Supplementary figures are contained in a Supplementary Data file. Source data for figures in the main text are provided online with the manuscript.

Code availability
Code to reproduce the main text figures are available with the source data. All the algorithms used are described in detail in the Supplementary Information.

References
74. Qin, D., Xia, Y. & Whitesides, G. M. Soft lithography for micro- and nanoscale patterning. *Nat. Protoc.* **5**, 491–502 (2010).
75. Edelstein, A., Amodaj, N., Hoover, K., Vale, R. & Stuurman, N. Computer control of microscopes using μManager. *Curr. Protoc. Mol. Biol.* **92**, 14.20.1–14.20.17 (2010).
76. Sourjik, V. & Berg, H. C. Functional interactions between receptors in bacterial chemotaxis. *Nature* **428**, 437–441 (2004).
77. Frymier, P. D., Ford, R. M., Berg, H. C. & Cummings, P. T. Three-dimensional tracking of motile bacteria near a solid planar surface. *Proc. Natl Acad. Sci. USA* **92**, 6195–6199 (1995).
78. Grognot, M. & Taute, K. M. A multiscale 3D chemotaxis assay reveals bacterial navigation mechanisms. *Commun. Biol.* **4**, 1–8 (2021).

Acknowledgements

Author contributions
H.H.M. and K.K. contributed equally to this work. H.H.M., K.K., B.B.M. and T.E. designed the research. H.H.M. and B.B.M. derived the theoretical bound with inputs from T.E. and K.K. H.H.M. performed the bacteria-tracking experiments. K.K. performed the single-cell FRET experiments. H.H.M., K.K. and T.E. validated the data. H.H.M., K.K., B.B.M. and T.E. discussed the data analysis. H.H.M. and K.K. performed the data analysis. H.H.M., K.K., B.B.M. and T.E. wrote the initial draft and all the revisions.

Competing interests
The authors declare no competing interests.

Additional information
Supplementary information The online version contains supplementary material available at https://doi.org/10.1038/s41567-021-01380-3.

Correspondence and requests for materials should be addressed to B. B. Machta or T. Emonet.

Peer review information *Nature Physics* thanks Lev Tsimring and the other, anonymous, reviewer(s) for their contribution to the peer review of this work.

Reprints and permissions information is available at www.nature.com/reprints.

nature portfolio

Corresponding author(s): Benjamin Machta and Thierry Emonet

Last updated by author(s): Aug 23, 2021

Reporting Summary

Nature Portfolio wishes to improve the reproducibility of the work that we publish. This form provides structure for consistency and transparency in reporting. For further information on Nature Portfolio policies, see our Editorial Policies and the Editorial Policy Checklist.

Statistics

For all statistical analyses, confirm that the following items are present in the figure legend, table legend, main text, or Methods section.

n/a	Confirmed	
☐	☒	The exact sample size (*n*) for each experimental group/condition, given as a discrete number and unit of measurement
☐	☒	A statement on whether measurements were taken from distinct samples or whether the same sample was measured repeatedly
☒	☐	The statistical test(s) used AND whether they are one- or two-sided *Only common tests should be described solely by name; describe more complex techniques in the Methods section.*
☒	☐	A description of all covariates tested
☒	☐	A description of any assumptions or corrections, such as tests of normality and adjustment for multiple comparisons
☐	☒	A full description of the statistical parameters including central tendency (e.g. means) or other basic estimates (e.g. regression coefficient) AND variation (e.g. standard deviation) or associated estimates of uncertainty (e.g. confidence intervals)
☒	☐	For null hypothesis testing, the test statistic (e.g. F, t, r) with confidence intervals, effect sizes, degrees of freedom and P value noted *Give P values as exact values whenever suitable.*
☐	☒	For Bayesian analysis, information on the choice of priors and Markov chain Monte Carlo settings
☒	☐	For hierarchical and complex designs, identification of the appropriate level for tests and full reporting of outcomes
☒	☐	Estimates of effect sizes (e.g. Cohen's *d*, Pearson's *r*), indicating how they were calculated

Our web collection on statistics for biologists contains articles on many of the points above.

Software and code

Policy information about availability of computer code

Data collection	MATLAB version 2018b and Micro-Manager versions 1.4 and 2.0 were used to control microscopes during data collection in this study.
Data analysis	Data analysis was performed in MATLAB version 2018b. All analysis algorithms are described in the Supplementary Information.

For manuscripts utilizing custom algorithms or software that are central to the research but not yet described in published literature, software must be made available to editors and reviewers. We strongly encourage code deposition in a community repository (e.g. GitHub). See the Nature Portfolio guidelines for submitting code & software for further information.

Data

Policy information about availability of data

All manuscripts must include a data availability statement. This statement should provide the following information, where applicable:
- Accession codes, unique identifiers, or web links for publicly available datasets
- A description of any restrictions on data availability
- For clinical datasets or third party data, please ensure that the statement adheres to our policy

Source data for the main text figures are provided online with the manuscript. Source data for the Supplementary Figures are contained in a Supplementary Data file.

Field-specific reporting

Please select the one below that is the best fit for your research. If you are not sure, read the appropriate sections before making your selection.

☒ Life sciences ☐ Behavioural & social sciences ☐ Ecological, evolutionary & environmental sciences

For a reference copy of the document with all sections, see nature.com/documents/nr-reporting-summary-flat.pdf

Life sciences study design

All studies must disclose on these points even when the disclosure is negative.

Sample size	No sample-size calculation was performed. Samples were collected until error bars on data points and parameters (standard error of the mean) were acceptable small.
Data exclusions	No data were excluded from the analyses.
Replication	Experiments were repeated across multiple days and bacterial cultures. Results were reproduced.
Randomization	Not relevant to this study. We did not test effects of interventions or perform hypothesis tests.
Blinding	Not relevant to this study. We did not test effects of interventions or perform hypothesis tests.

Reporting for specific materials, systems and methods

We require information from authors about some types of materials, experimental systems and methods used in many studies. Here, indicate whether each material, system or method listed is relevant to your study. If you are not sure if a list item applies to your research, read the appropriate section before selecting a response.

Materials & experimental systems

n/a	Involved in the study
☒	☐ Antibodies
☒	☐ Eukaryotic cell lines
☒	☐ Palaeontology and archaeology
☒	☐ Animals and other organisms
☒	☐ Human research participants
☒	☐ Clinical data
☒	☐ Dual use research of concern

Methods

n/a	Involved in the study
☒	☐ ChIP-seq
☒	☐ Flow cytometry
☒	☐ MRI-based neuroimaging